

Spatial and interannual variations of spring rainfall over eastern China in association with PDO–ENSO events

Xiaofei Wu^{1,2} · Jianguo Mao¹ 

Received: 21 March 2017 / Accepted: 7 November 2017 / Published online: 14 November 2017
© Springer-Verlag GmbH Austria, part of Springer Nature 2017

Abstract The spatio-temporal variations of eastern China spring rainfall are identified via empirical orthogonal function (EOF) analysis of rain-gauge (gridded) precipitation datasets for the period 1958–2013 (1920–2013). The interannual variations of the first two leading EOF modes are linked with the El Niño–Southern Oscillation (ENSO), with this linkage being modulated by the Pacific Decadal Oscillation (PDO). The EOF1 mode, characterized by predominant rainfall anomalies from the Yangtze River to North China (YNC), is more likely associated with out-of-phase PDO–ENSO events [i.e., El Niño during cold PDO (EN_CPDO) and La Niña during warm PDO (LN_WPDO)]. The sea surface temperature anomaly (SSTA) distributions of EN_CPDO (LN_WPDO) events induce a significant anomalous anticyclone (cyclone) over the western North Pacific stretching northward to the Korean Peninsula and southern Japan, resulting in anomalous southwesterlies (northeasterlies) prevailing over eastern China and above-normal (below-normal) rainfall over YNC. In contrast, EOF2 exhibits a dipole pattern with predominantly positive rainfall anomalies over southern China along with negative anomalies over YNC, which is more likely connected to in-phase PDO–ENSO events [i.e., El Niño during warm PDO (EN_WPDO) and La Niña during cold PDO (LN_CPDO)].

EN_WPDO (LN_CPDO) events force a southwest–northeast oriented dipole-like circulation pattern leading to significant anomalous southwesterlies (northeasterlies) and above-normal (below-normal) rainfall over southern China. Numerical experiments with the CAM5 model forced by the SSTA patterns of EN_WPDO and EN_CPDO events reproduce reasonably well the corresponding anomalous atmospheric circulation patterns and spring rainfall modes over eastern China, validating the related mechanisms.

1 Introduction

Eastern China is remarkably affected by the East Asian monsoon, with the major rainy season occurring typically in summertime (June–August) (Ding 1992). The complicated variations of the East Asian summer monsoon, especially the large interannual variability (e.g., Lau and Li 1984; Zhu and Yang 2003; Duan et al. 2013; Zhang et al. 2016), mean that the summer rainfall over eastern China has a great impact on the local agriculture and related economic activities. However, considerable rainfall also occurs during spring (March–May) due to the effects of the Tibetan Plateau (Wan and Wu 2007) and land–sea thermal contrast (Tian and Yasunari 1998). Spring is a transitional season between the winter and summer monsoons, with the climatological spring rainfall rate exhibiting a southward-increasing distribution from 0.2 to 8 mm day⁻¹ (Fig. 1a). Over southern China (SC, referring to the continental area south of 28° N and east of 105° E in present study), the spring rainfall accounts for as much as 30–40% of annual total rainfall (Wu and Mao 2016), with large interannual standard deviation that exceeds 2 mm day⁻¹ (Fig. 1b), leading to frequent severe floods and droughts over SC. Note that over the north of the Yangtze Basin, although the climatological spring rainfall is lower than that over SC

✉ Jianguo Mao
mgy@lasg.iap.ac.cn

¹ State Key Laboratory of Numerical Modeling for Atmospheric Sciences and Geophysical Fluid Dynamics (LASG), Institute of Atmospheric Physics, Chinese Academy of Sciences, P.O. Box 9804, Beijing 100029, China

² School of Atmospheric Sciences/Plateau Atmosphere and Environment Key Laboratory of Sichuan Province/Joint Laboratory of Climate and Environment Change, Chengdu University of Information Technology, Chengdu 610225, China

Fig. 1 **a** Climatology (color shading, mm day^{-1}) and **b** interannual standard deviation (color shading, mm day^{-1}) of spring (March–May) mean rainfall over eastern China based on the CMA rain-gauge station observations for the period 1958–2013

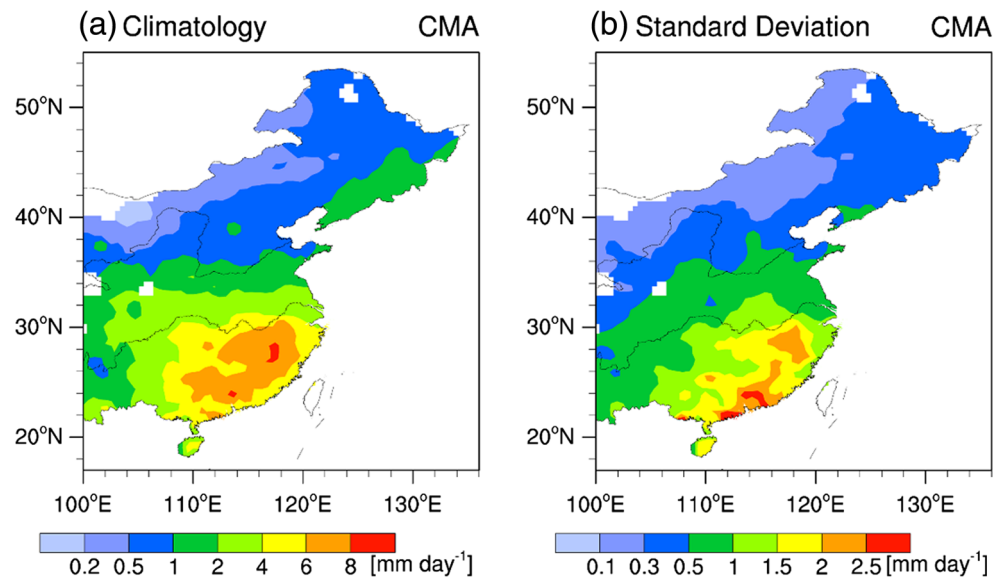


(Fig. 1a), the interannual standard deviation over most of northern China (Fig. 1b) is not small compared with the climatological spring rainfall, accounting for almost half of the climate-mean amounts (Fig. 1b). Such relatively large standard deviations over northern China imply that anomalous rainfall may have a huge impact on local socioeconomic development. For example, the spring drought in 1999 severely disrupted agricultural production over more than 1.03 million km^2 in northern China, leading to a reduction of the crop yields by 20–30% (Rong et al. 2008; An et al. 2014). Thus, understanding the mechanism of interannual variability and improving the seasonal forecasting skill of the spring rainfall over the entire area of eastern China are important for disaster prevention and mitigation.

There have already been some efforts to investigate the variability of spring rainfall and circulation over East Asia. The year-to-year variations of spring rainfall are found to be affected by many factors, such as the El Niño–Southern Oscillation (ENSO) (Wang et al. 2000; Wu et al. 2003; Feng and Li 2011; Chen et al. 2013a; Wu and Mao 2016), the Indian Ocean subtropical dipole (Feng et al. 2014b), Eurasian snow cover (Wu and Kirtman 2007; Zuo et al. 2012), and the Southern Hemisphere annular mode (Zheng and Li 2012; Zheng et al. 2015). Among all these factors, ENSO is the dominant variability in air–sea interaction on interannual timescales. However, the impact of ENSO on spring rainfall over eastern China is very complicated. Based on an empirical orthogonal function (EOF) analysis for the normalized spring rainfall anomalies from 1979 to 2004, Zuo and Zhang (2012) found that the most robust variability exists over a large area from the Yangtze to northern China (YNC, referring to the continental area between 32°N and 42°N and east of 105°E in the present study), especially around the middle and lower reaches of the Yellow River. They also noted that positive

spring rainfall anomalies over YNC are associated with positive sea surface temperature (SST) anomalies (SSTAs) in the tropical eastern Pacific and negative SSTAs in the tropical western Pacific in the previous winter and spring. A similar positive relationship between ENSO and the spring rainfall over the mid- and lower reaches of the Yangtze Basin has been derived by investigating the spatio-temporal evolution of ENSO-related seasonal rainfall anomalies in East Asia (Wu et al. 2003). The key system responsible for such rainfall anomalies is an anomalous low-level anticyclone over the western North Pacific (WNP), induced by large-scale equatorial heating anomalies and local air–sea interactions (Wang et al. 2000). In exploring the ENSO impacts on spring rainfall over SC, Feng and Li (2011) demonstrated that typical El Niño and El Niño Modoki have different influences, with El Niño Modoki leading to negative rainfall anomalies and typical El Niño resulting in positive rainfall anomalies. The above studies together provided some evidence that the anomalous spring rainfall in the entire region of eastern China is linked with ENSO. However, the interdecadal ENSO variability has been found and documented in some literatures, in which such decadal variability was suggested to originate from decadal changes in the tropics and midlatitudes (Gu and Philander 1997; Barnett et al. 1999; Tang et al. 2008). Thus, the interannual variability of spring rainfall in relation to ENSO may be modulated by decadal-scale fluctuations in extratropical SSTAs, such as the Pacific Decadal Oscillation (PDO) (Mantua et al. 1997). Wu and Mao (2016) identified the interdecadal modulation by the PDO of the relationship between ENSO and the South China spring rainfall (SCSR) in longer-term observational datasets. When ENSO and PDO are in-phase [i.e., El Niño events during warm PDO phases (EN_WPDO) and La Niña events during cold PDO phases (LN_CPDO)], the positive correlations between ENSO and

SCSR are enhanced significantly, with above-normal (below-normal) SCSR generally following EN_WPDO (LN_CPDO) events. In contrast, the ENSO–SCSR relationship becomes ambiguous when ENSO and PDO are out-of-phase (i.e., El Niño events during cold PDO phases and La Niña events during warm PDO phases). Therefore, similar interdecadal modulation of ENSO-related spring rainfall may also exist over YNC, with relatively robust relationships varying from epoch to epoch, although Gong and Wang (1998) pointed out that there is no stable relationship between ENSO and rainfall anomalies over eastern China in spring when longer-term datasets starting from 1880 are used.

In fact, as the dominant decadal variability in the Pacific, the PDO has prominent modulating effects on ENSO teleconnections with climate anomalies over various regions, such as North America (Gershunov and Barnett 1998), South America (Andreoli and Kayano 2005), Australia (Power et al. 1999), and South Asia (Krishnamurthy and Krishnamurthy 2014). For East Asia, the PDO is also suggested to modify the ENSO impacts on the winter monsoon (Wang et al. 2008; Kim et al. 2014; Wang et al. 2014), early summer monsoon (Chan and Zhou 2005; Mao et al. 2011; Wu and Mao 2017), and summer monsoon (Yoon and Yeh 2010; Chen et al. 2013b; Feng et al. 2014a). For example, Kim et al. (2014) suggested that the negative relationship between ENSO and the East Asian winter monsoon is significant only when the ENSO and PDO are in-phase, but there is no preference for positive or negative anomalies when the ENSO and PDO are out-of-phase. As mentioned above, a similar relationship between ENSO and spring rainfall over SC was observed by Wu and Mao (2016), who suggested the PDO modulating mechanism for the ENSO–SCSR relationship in which the PDO-forced circulation in the extratropical North Pacific modifies the spatial pattern and strength of the lower-tropospheric subtropical anticyclone over the western North Pacific.

Although in recent decades the spring rainfall anomalies over YNC in eastern China have exhibited a positive correlation with the ENSO-related SST anomalies in the tropical eastern Pacific (Zuo and Zhang 2012), does such a positive association between ENSO and YNC spring rainfall still hold over a much longer time period? Given that in our precious work (Wu and Mao 2016), we analyzed the modulating effects on ENSO-related spring rainfall only over SC, but does the PDO also modulate the ENSO-related spring rainfall over YNC? Furthermore, how is the spatial coherence of the temporal variability of rainfall anomalies over YNC related to that over SC in the entire eastern China? These questions need to be addressed. Therefore, the present study investigates the dominant modes of the spring rainfall anomalies over the entire eastern China and their temporal variations. The objective is to reveal how and to what extent the dominant modes are related to ENSO events under different PDO phases, and thus understand the physical mechanism of the synergistic

influence of the PDO and ENSO on spring rainfall over eastern China by examining how the PDO-forced circulation modifies the ENSO-induced circulation. It should be pointed out that the present study differs from our precious work (Wu and Mao 2016) in the following aspects. We extend the domain to the entire area of eastern China to examine whether the spring rainfall anomalies over the SC region themselves are constituted as a spatially independent pattern over the entire eastern China or how they are coherently teleconnected with rainfall anomalies over other regions. Moreover, we identify all dominant spatial patterns of spring rainfall anomalies over the entire eastern China on interannual timescale. Furthermore, we utilize the Community Atmosphere Model version 5.1 (CAM5) to carry out practically a series of numerical experiments rather than only use previous output of the Community Climate System Model (version 4, CCSM4) for “twentieth century” simulations to validate the diagnosed mechanisms responsible for the impacts of PDO–ENSO events on dominant spatial patterns of spring rainfall anomalies over eastern China.

Section 2 presents a brief description of datasets, analysis methods and numerical experiment design. Section 3 demonstrates the dominant modes of the spring rainfall anomalies over eastern China and their linkage with the PDO and ENSO. The physical mechanism responsible for the PDO modulation of the ENSO impact on the dominant modes is examined in Sect. 4. The resultant anomalous atmospheric circulation teleconnections forced by both PDO-related and ENSO-related SSTAs are validated using numerical experiments in Sect. 5. Finally, a summary and discussion are given in Sect. 6.

2 Data, methods, and modeling experiments

2.1 Observational and reanalysis datasets

Several observational and reanalysis datasets covering monthly rainfall, SSTs, and atmospheric circulation are used in the present study, and their details are listed in Table 1. Two different precipitation datasets and two different atmospheric reanalyses are utilized for a cross comparison. Usually, observational datasets based on surface stations and reanalysis products assimilating satellite-based information for recent decades are considered to have high accuracy and reliability. Thus, the rain-gauge precipitation from 756 stations in China provided by the China Meteorological Administration (CMA) and the Japan Meteorological Agency 55-year Reanalysis (JRA-55) (Kobayashi et al. 2015) are employed in this study. Meanwhile, because this study focuses on the decadal modulating effects of PDO, it is necessary to utilize observational and reanalysis datasets over as long a period as possible. However, both the CMA rain-gauge precipitation datasets and the JRA-55 reanalysis are available only from the

Table 1 Details of monthly datasets used in this study

	Resolution	Period of record	Source
Rain-gauge precipitation	756 stations	1958–2013	China Meteorological Administration
CRU TS 3.23 precipitation	0.5° × 0.5°	1920–2013	Harris et al. (2014)
JRA-55 reanalysis	1.25° × 1.25°	1958–2013	Kobayashi et al. (2015)
ERA-20C reanalysis	1° × 1°	1920–2010	Stickler et al. (2014)
HadISST1	1° × 1°	1920–2013	Rayner et al. (2003)

1950s. Therefore, the long-term gridded rainfall Time-Series (TS) version 3.23 provided by the Climate Research Unit (CRU) (Harris et al. 2014) and the twentieth century atmospheric reanalysis (ERA-20C) products provided by the European Centre for Medium-Range Weather Forecasts (ECMWF) (Stickler et al. 2014) are also used in this study for long-term validation. The Hadley Centre Sea Ice and SST dataset version 1.1 (HadISST 1.1) incorporates assimilated satellite-based information but also has long-term coverage (Rayner et al. 2003), and is therefore chosen as the SST dataset in this study.

2.2 Analysis methods

The climatological distribution of spring rainfall exhibits apparent differences in magnitude between SC and other areas (north of the Yangtze Basin) (Fig. 1a). Thus, the rainfall anomaly percentage calculated as the departure from the climatological mean for each station is used to reflect objectively the extent and magnitude of the rainfall anomaly. The climatological mean for each station or grid point is calculated as the long-term average of the base period from 1958 to 2013 for the CMA station-observation datasets or of the base period from 1920 to 2013 for the CRU datasets. EOF analysis is an objective and straightforward approach for identifying the spatio-temporal variability of a meteorological variable field. It is applied here to the spring rainfall anomaly percentages over the entire eastern China (east of 100° E) based on the CMA station-observed datasets for the period 1958–2013 and to those based on the CRU gridded datasets for the period 1920–2013, and gives the dominant EOF modes of spring rainfall anomalies over eastern China and the corresponding principal component (PC) time series. Note that the PC time series of a dominant EOF mode reflects how the spatial pattern of this mode varies with time, so each PC time series is actually considered as an index time series to measure the intensity of variable anomalies in the corresponding spatial pattern. Likewise, EOF analysis is also applied to the HadISST 1.1 data to recalculate the PDO index, following Mantua et al. (1997).

Two essential climatic oscillation indices, the Niño3.4 index and the PDO index, are employed in the present study. To ensure the consistency of the PDO and ENSO, the PDO and

the Niño3.4 indices are recalculated using the HadISST 1.1 dataset. The PDO index is defined as the leading PC from the EOF analysis of detrended monthly SST anomalies in the North Pacific Ocean (20°–60° N, 120° E–120° W) for the period 1920–2013 (Mantua et al. 1997). The data are detrended by subtracting the globally averaged SST anomalies (Zhang et al. 1997). The wintertime mean PDO index defined by the December–February (DJF) average is used to identify the PDO phases. Positive (negative) PDO years are determined when the 11-year running-mean DJF PDO index is above (below) zero. Because most ENSO events also tend to mature in wintertime (Rasmusson and Carpenter 1982), the area-averaged and detrended DJF Niño 3.4 SST anomaly over the region 5° S–5° N, 170–120° W is taken as an index to define ENSO events. An El Niño (La Niña) year is identified when the detrended DJF Niño 3.4 SST anomaly is greater than 0.55 °C (less than –0.55 °C), and this anomaly threshold is approximately equal to 0.6 standard deviations of the interannual variations of the Niño3.4 index. The Niño3.4 index is detrended to avoid the possible influence of phase shifts in the PDO (Gershunov and Barnett 1998). Based on the above classifications for PDO and ENSO, there are 26 El Niño and 26 La Niña events occurring along with two warm and two cold PDO epochs for the period 1920–2013, with the ENSO events that occur in different PDO epochs forming different PDO–ENSO combinations of PDO-related El Niño and La Niña events, as listed in Table 2. As in Wu and Mao (2016), these PDO-related El Niño and La Niña events can be further grouped into two categories based on whether PDO and ENSO are in-phase or out-of-phase. For the in-phase PDO–ENSO combinations, El Niño events occurring during warm PDO phases are abbreviated as EN_WPDO events, and La Niña events during cold PDO phases abbreviated as LN_CPDO events. The out-of-phase PDO–ENSO combinations are the El Niño events during cold PDO phases (EN_CPDO events) and La Niña events during warm PDO phases (LN_WPDO events).

Following Ihara et al. (2007), a contingency table is constructed to examine how and to what extent the dominant spatial patterns of the anomalous spring rainfall over eastern China are linked with El Niño and La Niña events under different PDO backgrounds. To depict the relationship clearly, the contingency table is divided into four 2 × 2 sub-tables to

Table 2 El Niño and La Niña years that are classified based on the PDO phase for the period 1920–2013. An ENSO year refers to wintertime in the calendar years when an El Niño or La Niña event peaks (e.g., year 1924 refers to the 1923/1924 winter, etc.). The ENSO years after 1958 are shown in italics

	Warm PDO	Cold PDO
El Niño	1924, 1926, 1931, 1940, 1941, 1942, 1978, 1980, 1983, 1987, 1988, 1992, 1998, 2003, 2005	1952, 1953, 1958, 1964, 1966, 1969, 1970, 1973, 1977, 2007, 2010
La Niña	1923, 1925, 1934, 1939, 1943, 1984, 1985, 1989, 1996, 1999, 2000, 2001, 2006	1950, 1951, 1955, 1956, 1965, 1968, 1971, 1974, 1976, 2008, 2009, 2011, 2012

calculate the numbers of positive (negative) PC1 and positive (negative) PC2 occurrences for in-phase PDO–ENSO (EN_WPDO and LN_CPDO) and out-of-phase PDO–ENSO (EN_CPDO and LN_WPDO) events. For each 2×2 sub-table, Fisher's exact test is utilized to examine the statistical significance of the association between the PDO–ENSO events and the dominant modes of the anomalous spring rainfall over eastern China. Fisher's exact test (see Appendix A for details) can compute the exact probability distribution for a set of contingency tables under the constraint of equal row and column totals, and thus it is a non-parametric test (Conover 1980).

The influence of the different PDO–ENSO events on rainfall anomalies during the subsequent spring (i.e., when ENSO decays) is then examined. Unless otherwise stated, ENSO-related circulation and rainfall anomalies in the following text refer to those in the spring following the peak of the PDO–ENSO events. Because the SSTA distributions and the resultant atmospheric responses of an EN_WPDO event tend to be opposite to those of a LN_CPDO event (as discussed below), for brevity, we use the composite differences between EN_WPDO and LN_CPDO events to summarize the anomalous oceanic and atmospheric patterns associated with the EN_WPDO and LN_CPDO events. Such composite differences of EN_WPDO minus LN_CPDO (abbreviated as in-phase composite differences) can clearly represent the resultant circulation anomalies during EN_WPDO events, with reverse situations for LN_CPDO events. Similarly, for the out-of-phase PDO–ENSO events, the anomalous conditions in SST and atmospheric circulation associated with EN_CPDO are highlighted by the composite differences of EN_CPDO minus LN_WPDO, with opposite situations for LN_WPDO events.

The statistical significance of the composite differences is estimated by bootstrap resampling (Efron 1982; Gershunov and Barnett 1998). Bootstrap resampling is a nonparametric statistical method that is superior to other statistical distributions and is applicable to both small and large sample sizes. The composite difference at each grid point is computed repeatedly 5000 times using the resampled variable series derived from random permutations of the original series. The 0.025th and 0.975th quantiles are the lower and upper bounds of the bootstrapped 95% confidence interval.

2.3 Model simulations

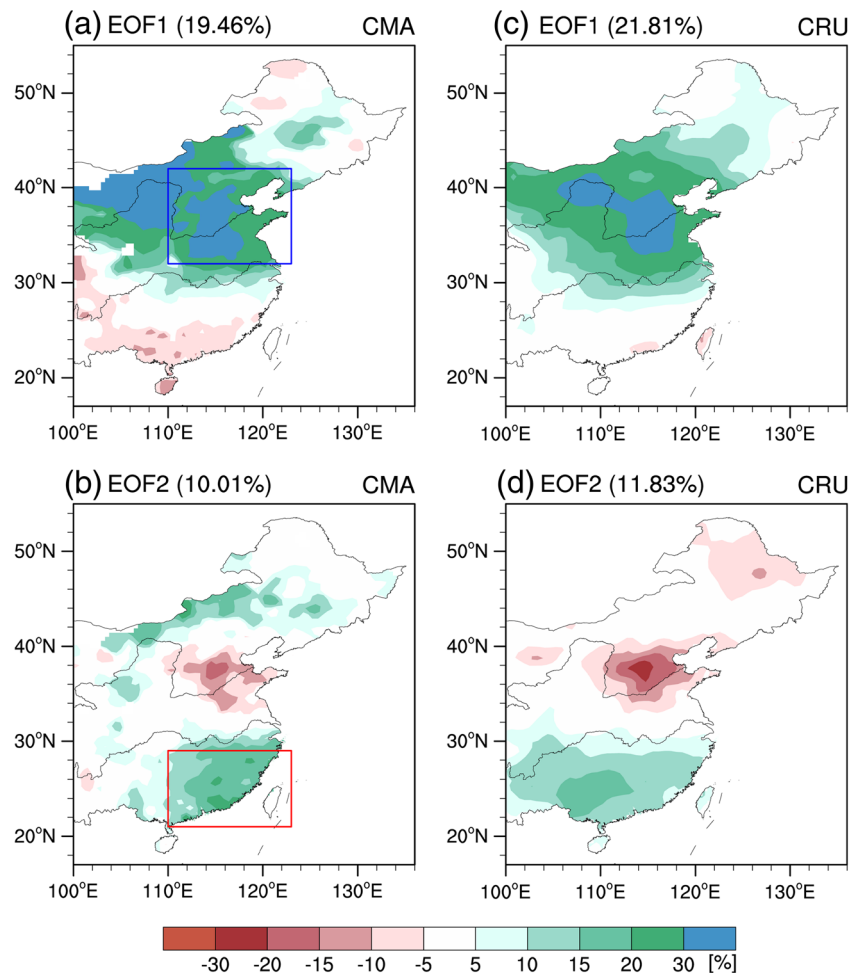
To verify the importance of the extratropical SSTAs in the mid-latitude North Pacific associated with the PDO in modifying the ENSO-related SSTA patterns from the tropical Pacific to the extratropical North Pacific and their resultant forcing to induce anomalous atmospheric circulation teleconnections, we perform numerical experiments using the Community Atmosphere Model version 5.1 (CAM5) (Conley et al. 2012), the atmospheric component of the Community Earth System Model (CESM). The model configuration used for this study has a horizontal resolution of 1.9° latitude \times 2.5° longitude and a sigma–pressure vertical coordinate with 30 levels from the surface to the top at 2.255 hPa, which reproduces reasonably well the climatological distribution of spring rainfall over East Asia (Li et al. 2015). One control experiment and two sensitivity experiments are run using different SST patterns as varying surface boundary conditions. The control experiment (referred to as CAM5-CTRL) is forced by the climatological mean annual cycle of SST. The first sensitivity experiment is forced by the climatological mean annual cycle of SSTs with the composite monthly varying SSTAs of EN_WPDO events superimposed only from December to June, to simulate the in-phase PDO–ENSO impact (referred to as CAM5-In-phase). The other sensitivity experiment is forced in the same way except that the SSTAs of EN_CPDO events are superimposed to simulate the out-of-phase PDO–ENSO situations (referred to as CAM5-Out-of-phase). All three experiments are run continuously for 35 years. To remove the possible impact of initialization and transients on the model results, only the output for the last 30 years are analyzed in this study.

3 Spatio-temporal variability of spring rainfall anomalies over eastern China in relation to PDO and ENSO

3.1 Spatio-temporal variability of anomalous rainfall

Figure 2a, b shows the spatial patterns of the first two leading EOFs of the spring rainfall anomaly percentages over eastern China derived from CMA rain-gauge data for the period

Fig. 2 Spatial patterns of the first two leading EOFs of the spring rainfall anomaly percentages over eastern China for **a** EOF1 and **b** EOF2 based on the CMA rain-gauge station observations for the period 1958–2013. The loadings (unit %) are scaled by one standard deviation of the corresponding PC. The percentage in parenthesis at the top of each panel refers to the variance explained by the mode. **c, d** Same as **a** and **b** but based on the CRU datasets for the period 1920–2013

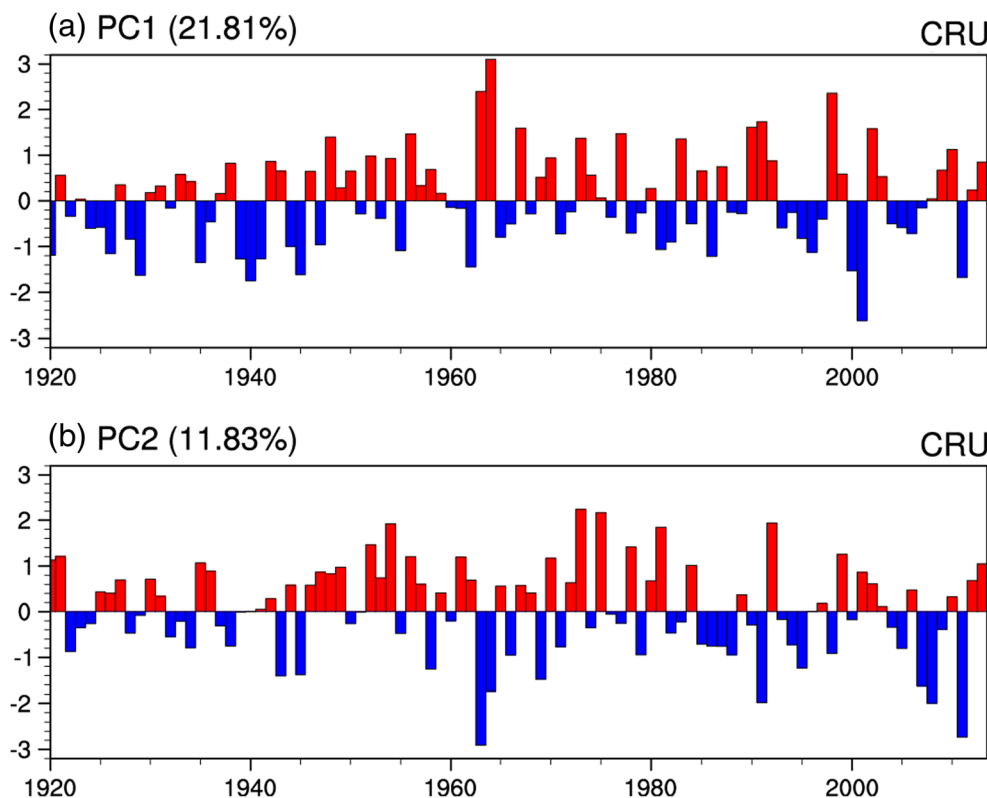


1958–2013, with the first mode (EOF1) and second mode (EOF2) accounting for 19.46 and 10.01% of the total variance, respectively. Each of these two modes is separated from the subsequent mode based on the test of statistical significance proposed by North et al. (1982).

EOF1 is dominated by positive anomalies over the middle and lower reaches of the Yellow River from the Yangtze to northern China (YNC), with weak negative anomalies confined only to the most southern portion of SC (Fig. 2a), similar to that identified by Zuo and Zhang (2012). In contrast, the EOF2 mode shows a north–south oriented dipole structure with predominant positive rainfall anomalies over SC in conjunction with negative anomalies over the lower reaches of the Yellow River in YNC (Fig. 2b). To substantiate the robustness of such dominant spatial patterns and their temporal variations for a longer time period, the same EOF analysis is applied to the CRU rainfall data from 1920 to 2013. The monopole structure of the CRU EOF1 (Fig. 2c) with coherent positive rainfall anomalies over YNC is more striking than the same EOF1 pattern (Fig. 2a) derived from CMA records for a relatively shorter period. Similarly, the dipole pattern of EOF2 (Fig. 2d) becomes more evident than that in Fig. 2b, with

distinctly opposite rainfall anomalies over SC and over the lower Yellow River Basin. This demonstrates that the EOF1 and EOF2 modes indeed represent two fundamental spatial patterns of spring rainfall variability over eastern China. Such high similarities between the dominant EOF structures derived from the two datasets also provide crucial evidence that the CRU datasets are reliable for describing the spatio-temporal variability of the spring rainfall anomalies over eastern China. The spatial pattern of a leading EOF mode better represents large, coherent rainfall variations over an analyzed domain, and the time-varying amplitude of this spatial pattern can be reflected by the corresponding PC time series. The longer normalized PC1 and PC2 time series from the CRU datasets are therefore used to represent the temporal variations of the two leading EOF modes (Fig. 3) because the longer-term time series is more suitable for detecting interannual variations of rainfall and their interdecadal modulations associated with the PDO. As shown in Fig. 3, the temporal evolutions of both PC1 and PC2 exhibit distinct year-to-year variations with large amplitudes greater than one standard deviation occurring in many years. Such strong interannual fluctuations of PC1 are found to be associated with ENSO events,

Fig. 3 The normalized Principal component (PC) time series for **a** PC1 and **b** PC2 corresponding to EOF1 and EOF2 based on the CRU datasets for the period 1920–2013. The percentage in parenthesis at the top of each panel refers to the variance explained by the mode



with the correlation coefficient between PC1 and the Nino3.4 index being 0.23, which is statistically significant at the 95% confidence level. However, the correlation between PC2 and Nino3.4 index is only 0.08, which is not statistically significant. But this does not mean that the interannual variability of the EOF2 mode has nothing to do with ENSO events; rather, the interannual relationship between PC2 and ENSO may undergo interdecadal changes. The spatial pattern of EOF2 (Fig. 2b, d) bears a strong resemblance to the composite distribution of spring rainfall anomalies over SC under the in-phase PDO–ENSO combination, as reported by Wu and Mao (2016), with significant positive rainfall anomalies both occurring over SC. Therefore, the interannual variability of PC1 and PC2 modulated by the PDO is explored below.

3.2 Leading EOF modes linked with the PDO and ENSO

To examine the link between the interannual variations of the dominant EOF modes with ENSO events under different PDO backgrounds, the numbers of positive or negative PC1 or PC2 years are counted up separately for the four PDO–ENSO combinations (Table 3). For example, the numbers of positive PC1 occurring in EN_WPDO years, EN_CPDO years, LN_WPDO years, and LN_CPDO years are 8, 6, 8, and 3, respectively, as shown in the first column of the PC1 cells in Table 3.

Using the different combinations of ENSO events with PDO backgrounds, the contingency table is again considered

as comprising two principal groups of in-phase and out-of-phase PDO–ENSO events, as shown in Table 3. The contingency table is divided into four 2×2 sub-tables: the sub-tables of in-phase events vs. PC1 (upper left sub-table in Table 3), in-phase events vs. PC2 (upper right sub-table in Table 3), out-of-phase events vs. PC1 (lower left sub-table in Table 3) and out-of-phase events vs. PC2 (lower right sub-table in Table 3).

Table 3 Contingency table for the numbers of positive and negative normalized PC1 and PC2 (corresponding to EOF1 and EOF2 of anomalous spring rainfall over eastern China) vs. four different PDO–ENSO events for the period 1920–2013. The *p* value shows the statistical significance of the association of anomalous PCs with the in-phase PDO–ENSO (EN_WPDO and LN_CPDO) or out-of-phase PDO–ENSO (EN_CPDO and LN_WPDO) events in each 2×2 sub-table, with statistical significance at the 90 or 95% confidence level indicated by italics

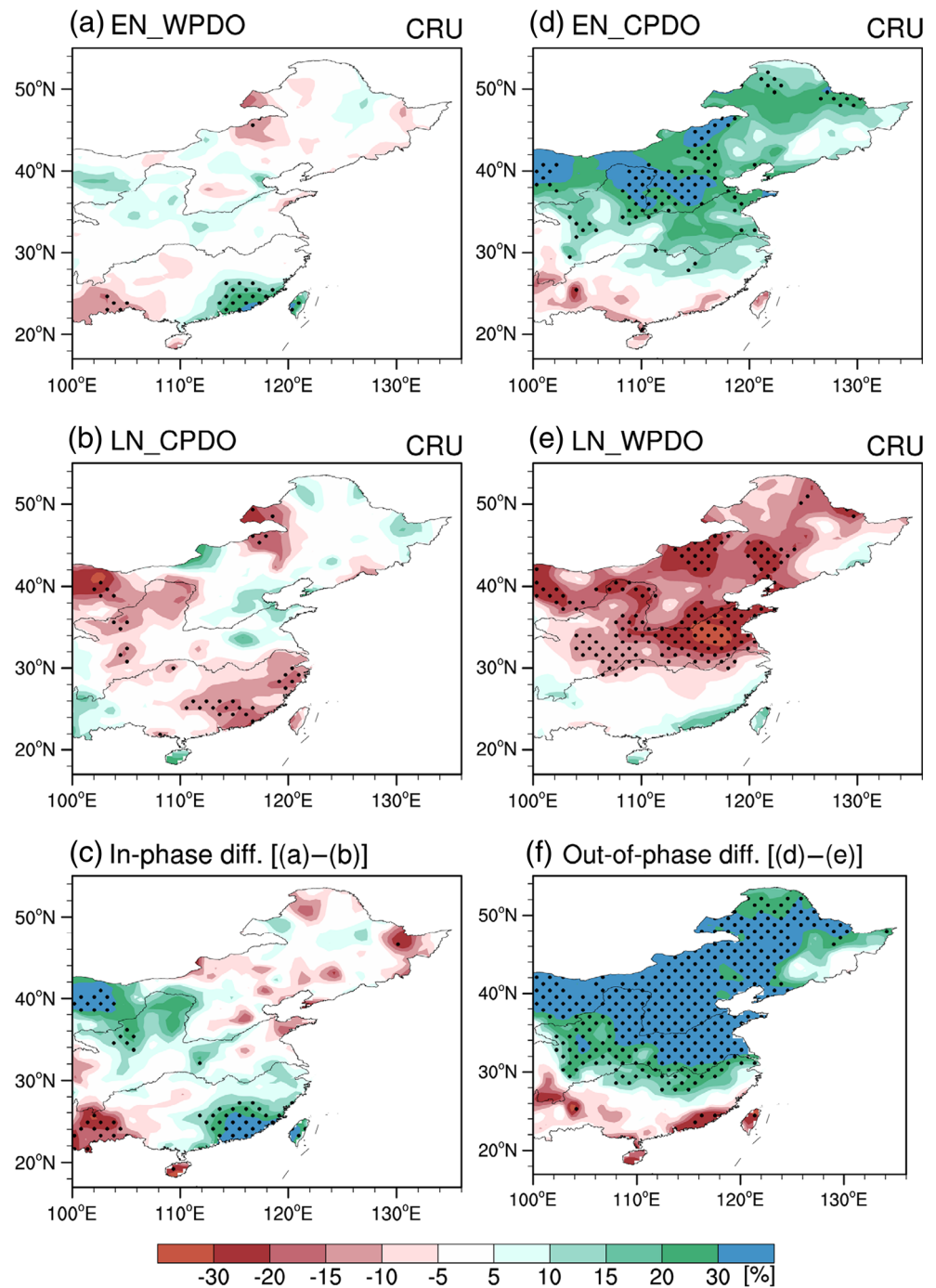
		PC1			PC2		
		+	-	Total	+	-	Total
In-phase	EN_WPDO	8	7	15	10	5	15
	LN_CPDO	6	7	13	4	9	13
	Total	14	14	28	14	14	28
		<i>p</i> = 0.50			<i>p</i> = 0.064		
Out-of-phase	EN_CPDO	8	3	11	5	6	11
	LN_WPDO	3	9	12	7	5	12
	Total	11	12	23	12	11	23
		<i>p</i> = 0.030			<i>p</i> = 0.42		

For the sub-table of in-phase events vs. PC1, the numbers of positive PC1 and PC2 years are nearly equal for both EN_WPDO and LN_CPDO, so that Fisher's exact test gives the probability of such a frequency distribution as 0.50, indicating that positive or negative PC1 preferences are not dependent on EN_WPDO and LN_CPDO events. That is, the dominant EOF1 mode of the anomalous spring rainfall pattern over YNC (as in Fig. 2a, c) is less likely related to the in-phase PDO–ENSO situations. On the contrary, as shown in the sub-table of the in-phase categories vs. PC2, the number of positive (negative) PC2 years is much greater than that of negative (positive) PC2 years for the EN_WPDO (LN_CPDO). Note that 10 out of 15 EN_WPDO events are followed by positive PC2, while 9 out of 13 LN_CPDO events correspond to negative PC2. Consequently, the probability of such a frequency distribution occurring randomly is 0.064, nearly reaching the 0.05 significance level, indicating that a positive association exists between PC2 and the in-phase PDO–ENSO events. In other words, the dominant EOF2 mode of the anomalous spring rainfall pattern over both SC and the lower reaches of the Yellow River (as in Fig. 2b, d) is more likely a result of the EN_WPDO and LN_CPDO events. For the out-of-phase events related to PC1 and PC2, there are 8 out of 11 EN_CPDO events corresponding to positive PC1, while 9 out of 12 LN_WPDO events are followed by negative PC1. The probability of the frequency distribution for PC1 is 0.030, exceeding the 0.05 significance level. Thus, the EOF1 mode (Fig. 2a, c) is more likely related to the out-of-phase PDO–ENSO conditions, with the EN_CPDO (LN_WPDO) events favoring positive (negative) spring rainfall anomalies over YNC. In contrast, the distribution probability of frequency for PC2 is 0.42, which is not statistically significant, indicating that the EOF2 mode (Fig. 2b, d) is less likely to be associated with the out-of-phase PDO–ENSO events.

To further confirm the association between the in-phase PDO–ENSO events and PC2, the composite anomalies of spring rainfall for EN_WPDO years and LN_CPDO years are shown in Fig. 4a, b, respectively. Following the EN_WPDO events, the spring rainfall exhibits significant positive anomalies over SC, but none over the other regions of eastern China (Fig. 4a), which agrees well with the spatial EOF2 pattern (Fig. 2d). Conversely, negative rainfall anomalies appear over SC in the spring following LN_CPDO events (Fig. 4b), with the EOF2 pattern reversed. Note that the composite differences of these two in-phase PDO–ENSO events (Fig. 4c) reproduce more clearly the EOF2 pattern. The relationship between out-of-phase PDO–ENSO events and PC1 is similarly confirmed. The EN_CPDO events induce significantly positive rainfall anomalies over YNC (Fig. 4d) and LN_WPDO events force reversed rainfall anomalies over the same region (Fig. 4e), corresponding to the EOF1 pattern with positive and negative rainfall anomalies (Fig. 2c), respectively.

The above comparisons demonstrate that the PDO can actually modify the relationship between ENSO and the spring rainfall over eastern China. When the PDO and ENSO are in-phase, the ENSO is significantly positively correlated with the spring rainfall over SC, corresponding to the EOF2 pattern of spring rainfall anomalies over eastern China. When PDO and ENSO are out-of-phase, the area with significantly positive correlations is displaced to the YNC, corresponding to the EOF1 pattern of spring rainfall anomalies over eastern China. Again, such a modulating effect can be further verified using box-and-whisker plots to compare the statistical distributions of year-by-year rainfall anomalies over SC and YNC for the four different PDO–ENSO events. The box-and-whisker plot is a non-parametric way of graphically depicting groups of numerical data through their quartiles, which can conveniently display variations in samples of a statistical population without making any assumptions of underlying statistical distribution (Hoaglin et al. 1983). The time series of area-averaged spring rainfall anomaly percentage over YNC (blue rectangle in Fig. 2a) or over SC (red rectangle in Fig. 2b) are calculated as statistical samples for CRU data from 1920 to 2013 and for CMA data from 1958 to 2013. These two areas are selected to represent EOF1 and EOF2 patterns, respectively, because the larger loadings of the spring rainfall anomaly percentages are mostly located in these two areas. As shown in Fig. 5, for in-phase PDO–ENSO events, the 25th percentile line of the SC rainfall anomaly percentage is above zero for EN_WPDO events, with both median and mean values of rainfall anomaly percentage greater than zero. The 75th percentile line is however below zero for LN_CPDO events, with both median and mean values of rainfall anomaly percentage less than zero. Thus the above-normal (below-normal) spring rainfall over SC tends to follow EN_WPDO (LN_CPDO) events. As for the anomalous rainfall over YNC, in contrast, the 75th percentile of the YNC rainfall anomaly percentage is greater than zero, while the 25th percentile is less than zero for both EN_WPDO and LN_CPDO categories. Note that the mean value of the YNC rainfall anomaly percentage for each of these two categories is close to zero. This suggests that the preference of spring rainfall anomalies over YNC becomes less deterministic under the in-phase PDO–ENSO situations. For out-of-phase events, EN_CPDO events appear to favor positive rainfall anomalies over YNC, which can be identified by the 25th percentiles of the YNC rainfall anomaly percentage above 0, while LN_WPDO events are conducive to negative rainfall anomalies over YNC with the 75th percentiles below 0. For rainfall anomalies over SC, however, no positive or negative preferences are found in either the EN_CPDO or LN_WPDO categories. Evidently, the interannual variability of the spring rainfall over eastern China is indeed linked with ENSO events, with such ENSO-related spring rainfall mostly occurring over YNC and SC as indicated by the corresponding dominant EOF1 and EOF2 modes. The association of each

Fig. 4 Composite distributions of detrended spring (March–May) rainfall anomaly percentage (shading, %) for the period 1920–2013 based on CRU datasets. Left panels show the in-phase PDO–ENSO events for **a** EN_WPDO and **b** LN_CPDO and **c** the differences between **a** and **b**. Right panels demonstrate the out-of-phase events for **d** EN_CPDO and **e** LN_WPDO and **f** the differences between **d** and **e**. The stippling denotes the anomalies being statistically significant at the 95% confidence level



dominant EOF mode with ENSO is significantly modulated by PDO, with the EOF2 (EOF1) mode more likely resulting from in-phase (out-of-phase) PDO–ENSO events. Specifically, the EN_WPDO (LN_CPDO) events tend to favor positive (negative) spring rainfall anomalies over SC and negative (positive) spring rainfall anomalies over the lower reaches of the Yellow River in YNC, while the EN_CPDO (LN_WPDO) events favor positive (negative) spring rainfall anomalies over YNC.

4 PDO modulation of ENSO-related SST and circulation anomalies

4.1 SST anomalies

To uncover the mechanism for the PDO modulation of the effects of ENSO on the spring rainfall anomalies over eastern China, composite analyses are produced by comparing the SST and circulation anomalies between the in-phase and

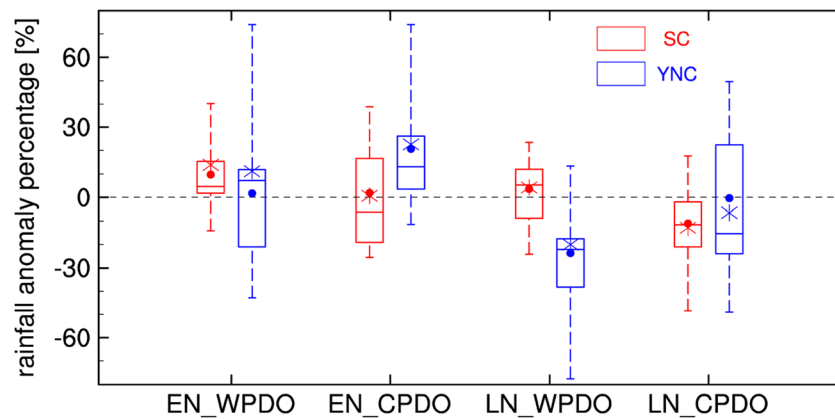


Fig. 5 Box and whisker plots of area-averaged rainfall anomaly percentage for the period 1920–2013 based on CRU datasets with respect to the four different PDO–ENSO events (shown as abscissa) over SC (indicated by red color, with the area to be averaged as the red rectangle shown in Fig. 2b) and over YNC (indicated by blue color, with the area to be averaged as the blue rectangle shown in Fig. 2a). The normal rainfall is indicated by horizontal dashed line. The lower and

upper boundaries of each box represent the 25th and 75th percentiles of the rainfall anomaly percentage. The solid horizontal line within each box shows the median of the rainfall anomaly percentage, while the circle within the box denotes the mean. The lower and upper whiskers for the minimum and maximum of rainfall anomaly percentage. Note that the asterisk in the box indicates the mean of the rainfall anomaly percentage for the period 1958–2013 based on the CMA rain-gauge station data

out-of-phase categories of PDO–ENSO combinations. It is well known that the typical SSTA distribution of an El Niño (La Niña) event is characterized by strong positive (negative) anomalies over the central and eastern equatorial Pacific in conjunction with weak negative (positive) anomalies over the extratropical North Pacific. A similar SSTA pattern occurs in a warm (cold) PDO year, except that the magnitude of PDO-based SSTAs in the mid-latitude North Pacific is larger than that in the equatorial Pacific (Mantua et al. 1997). Therefore, if El Niño events occur in warm PDO phases, the resultant EN_WPDO events would be characterized by both enhanced positive SSTAs in the equatorial Pacific and enhanced negative SSTAs in the mid-latitude North Pacific (Fig. 6a), due to in-phase superposition of SSTAs. In the other in-phase category, the LN_CPDO events exhibit a similarly enhanced SSTA pattern to the EN_WPDO, but with reversed signs for the SSTAs (Fig. 6b). As mentioned above, the EN_WPDO and LN_CPDO in-phase PDO–ENSO events exhibit distinctly opposite polarities in SSTA distribution (Fig. 6a, b), so that the EN_WPDO minus LN_CPDO differences (Fig. 6c) can simply represent the anomalous condition of EN_WPDO events, with the opposite situation for LN_CPDO events. In addition, such differences in SSTAs between EN_WPDO and LN_CPDO categories can highlight the in-phase superposed effects that force anomalous circulation (as discussed below). In contrast, for the out-of-phase PDO–ENSO categories, the ENSO-related SSTAs and PDO-related SSTAs tend to cancel each other out. Therefore, if El Niño events occur during a cold PDO phase, the resultant EN_CPDO events have weakened positive SSTAs over the equatorial Pacific and also weakened positive SSTAs over the North Pacific (Fig. 6d), because the amplitude of SSTAs over the equatorial Pacific for El Niño events is usually larger

than that for cold PDO episodes but opposite over the mid-latitude North Pacific. The LN_WPDO events exhibit a similar weakened SSTA distribution to the EN_CPDO events, but with reversed signs for SSTAs (Fig. 6e). Thus, the out-of-phase superimposed effects in SSTAs (Fig. 6f) along with the resultant circulation anomalies (as discussed below) are also highlighted by the composite differences between EN_CPDO and LN_WPDO events.

The in-phase composite SSTA pattern (Fig. 6c), as modified by the PDO-related SST anomalies, exhibits significantly enhanced positive anomalies over the central and eastern equatorial Pacific and also enhanced negative anomalies over the mid-latitude North Pacific. But for the out-of-phase composite, the SSTAs in the equatorial Pacific are much weaker, with only some positive anomalies remaining over the central equatorial Pacific (Fig. 6f), similar to the features of El Niño Modoki (Ashok et al. 2007) or central Pacific El Niño (Kao and Yu 2009). The central Pacific El Niños are observed to occur more frequently in recent decades (McPhaden et al. 2011), with a systematic shift of more frequent occurrences of central Pacific El Niños versus eastern Pacific El Niños during 2000–2010 relative to 1980–1999. McPhaden et al. (2011) further attributed the systematic shift to changes in background state because of the asymmetric spatial structures of central Pacific El Niños and eastern Pacific El Niños. Such a systematic shift may be associated with the decadal transition in PDO phases as shown in Wu and Mao (2016), who noted that the PDO experiences a phase transition of warm PDO to cold PDO within the period 1980–2010. As such, the in-phase composite SSTA pattern (Fig. 6c) actually represents the typical features of eastern Pacific El Niños, while the out-of-phase composites (Fig. 6f) mostly reflect the situations of central Pacific El Niños. Note that in the WNP, the out-of-

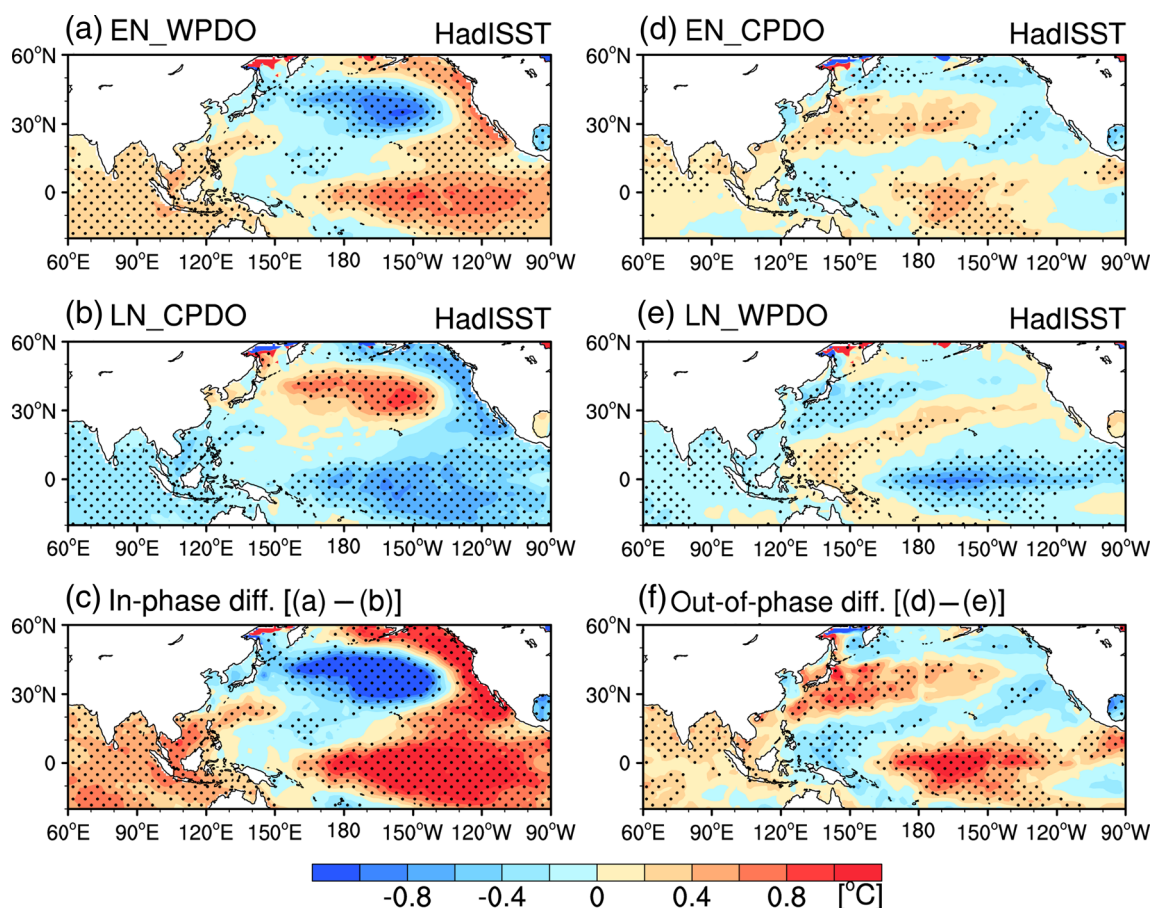


Fig. 6 Same as Fig. 4 but for the SST anomalies for the period 1920–2013

phase composites show a long belt of significantly positive SSTAs extending from the coast of East Asia to the central North Pacific, accompanied by significantly negative anomalies over the western equatorial Pacific (Fig. 6f), but the positive SSTA anomalies of the in-phase composites are only significant in the South China Sea and northern part of the Philippine Sea (Fig. 6c). These different distributions between in-phase and out-of-phase composite SSTAs, resulting from the modulation of PDO-related SSTAs, would certainly force different circulation anomalies.

4.2 Circulation anomalies

To explore the circulation anomalies forced by the in-phase and out-of-phase composite SSTAs, the sea-level pressure (SLP) and lower tropospheric winds together with moisture conditions are examined. For the in-phase composites, a strong anomalous anticyclone associated with positive SLP anomalies dominates the WNP, accompanied by a simultaneously enhanced Aleutian low over the North Pacific (Fig. 7a, d). The strong anomalous anticyclone is forced by the enhanced SSTAs over the central and eastern equatorial Pacific (Fig. 6c). As suggested by Wang et al. (2000), the

anomalous WNP anticyclone results from a Rossby-wave response to suppressed convective heating, which is induced by both the in situ ocean surface cooling and the subsidence forced remotely by the central Pacific warming. The in-phase superposition of PDO and ENSO enhances the positive SSTAs in the central and eastern equatorial Pacific (Fig. 6c) that excite a westward propagating Rossby wave subsiding over the WNP, and then strengthen the strong anticyclone over the WNP (Fig. 7a, d). Moreover, associated with the intensified negative SSTAs over the central North Pacific (Fig. 6c), a strong and westward-extended Aleutian Low is present over the North Pacific (Fig. 7a, d). The enhanced Aleutian Low extends westward to East Asia, and the anomalous anticyclone contracts away from the coastal region of East Asia. As a result, the anomalous WNP anticyclone is confined to southern parts of the South China Sea and east of the Philippines, resulting in strong anomalous southwestlies only over SC (Fig. 7a, d). Consequently, such southwesterly anomalies bring large amounts of water vapor to SC, as indicated by the southwesterly anomaly of the vertically integrated vapor flux over SC (Fig. 8a, d). The anomalous vapor flux converges over SC (Fig. 8a, d), leading to above-normal rainfall over SC (Fig. 4c), in agreement with the

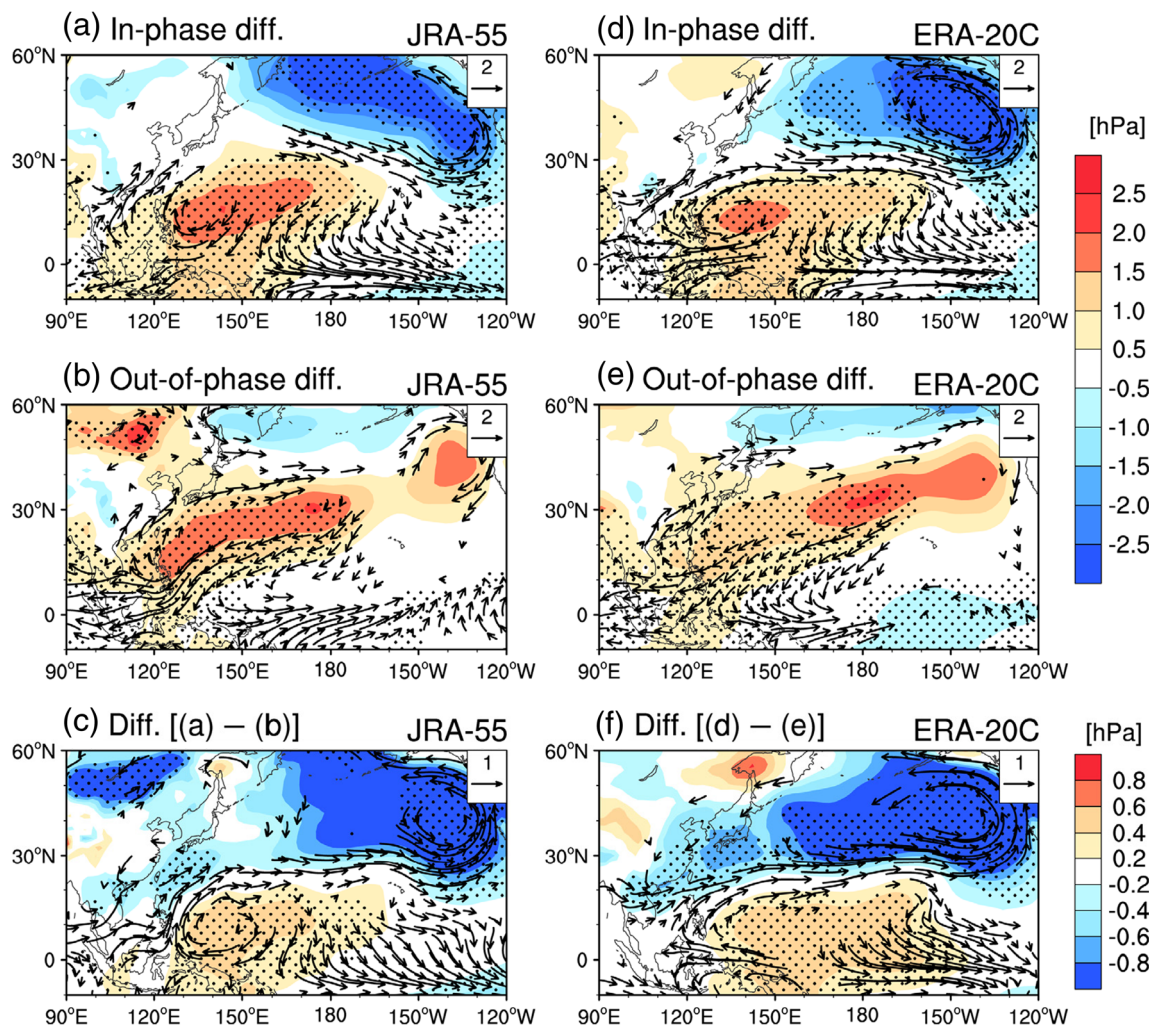


Fig. 7 Composite differences of spring (March–May) SLP (shading, hPa) and 850-hPa wind (vectors, m s^{-1}) based on the JRA-55 reanalysis for the period 1958–2012 **a** between the in-phase PDO–ENSO events, EN_WPDO minus LN_CPDO; **b** between the out-of-phase PDO–ENSO events, EN_CPDO minus LN_WPDO; and **c** between in-phase and out-of-phase conditions [i.e., **a** minus **b**]. Stippling denotes SLP anomalies

statistically significant at the 95% confidence level. Vectors are only shown if at least one of the anomalous zonal and meridional wind components is statistically significant at the 95% confidence level. **d–f** Same as **a–c** but based on the ERA-20C reanalysis data for the period 1920–2010

EOF2 pattern of spring rainfall anomalies over eastern China (Fig. 2b, d).

The circulation anomalies of the out-of-phase composite are significantly different from those of the in-phase composite. In response to the weakened SSTAs in the equatorial Central Pacific (Fig. 6f), there is a weakened anticyclone over the WNP (Fig. 7b, e). Although the strength of the WNP anticyclone in the out-of-phase composite is somewhat weaker than that in the in-phase composite (Fig. 7a, d), it extends northeastward to connect with the positive SLP anomalies over the eastern North Pacific (Fig. 7b, e), which are associated with the cold PDO-related positive SSTAs over the North Pacific (Fig. 6f). More importantly, in response to the significantly positive SSTAs from the coast of East Asia to the central North Pacific, the anomalous WNP anticyclone also extends northward to eastern and northern China (Fig. 7b, e). As a

result, large amounts of water vapor are transported to the YNC regions as indicated by the anomalous vertically integrated vertical vapor (Fig. 8b, e). Abundant water vapor converges over YNC (Fig. 8b, e), resulting in above-normal rainfall over those regions (Fig. 4f), corresponding to the EOF1 pattern of spring rainfall anomalies over eastern China (Fig. 2a, c).

In addition, the differences of SLP and 850-hPa winds between in-phase and out-of-phase composites are shown in Fig. 7c, f. A dipole-like anomalous circulation is present over the Pacific and East Asia, characterized by an anomalous anticyclone over the equatorial western Pacific and a cyclone over the North Pacific. The strong anomalous cyclone over the North Pacific that extends southwestward to East China together with the anomalous anticyclone over east of the Philippines are the typical characteristics of warm PDO-related circulation anomalies (Mantua et al. 1997). As a result,

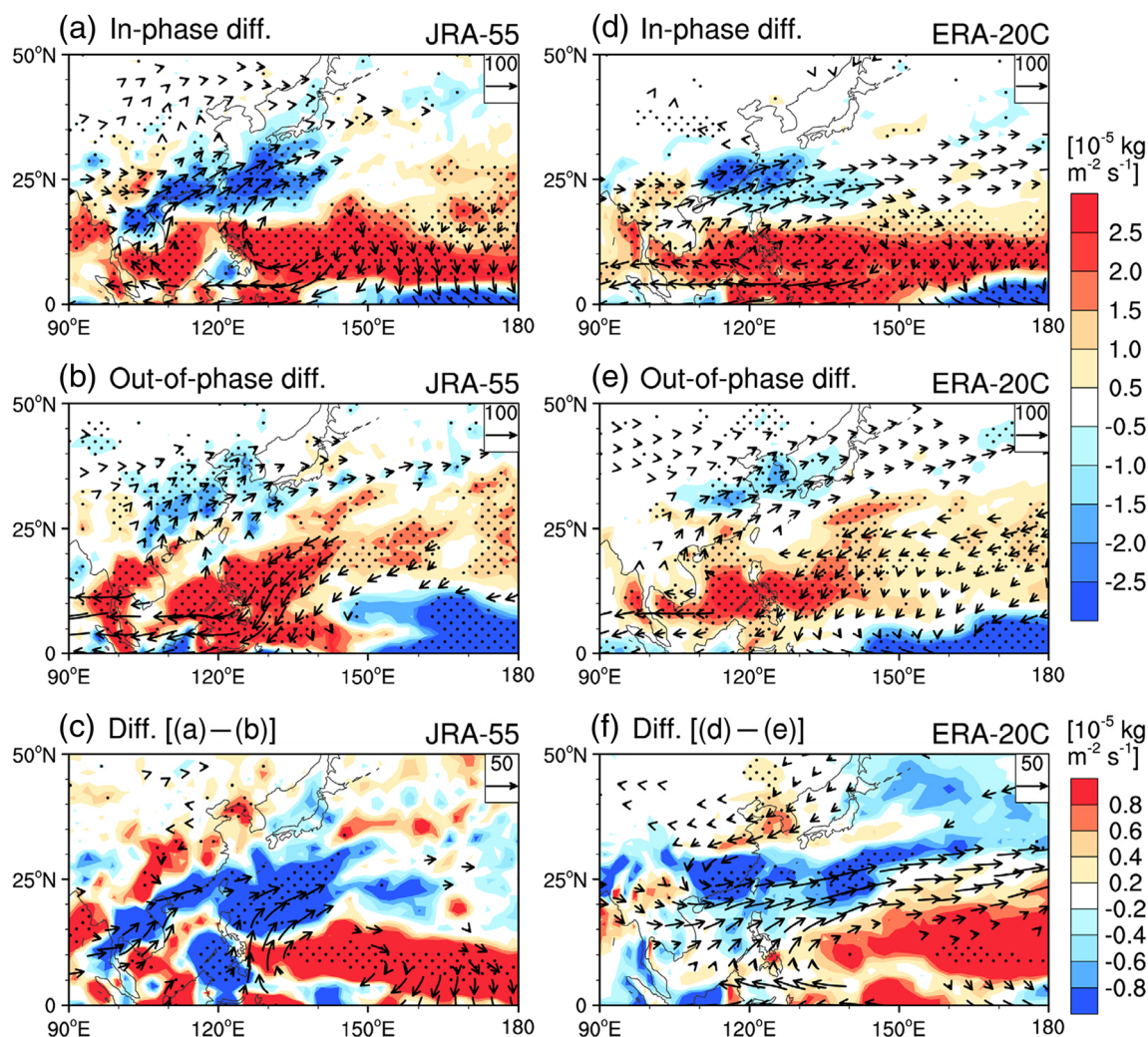


Fig. 8 Same as Fig. 7 but for the vertically integrated water vapor flux (vectors, $\text{kg m}^{-1} \text{s}^{-1}$) and its divergence (shading, $10^{-5} \text{ kg m}^{-2} \text{s}^{-1}$)

anomalous northeasterlies prevail over YNC and converge with the anomalous southwesterlies over SC and north of the South China Sea (Fig. 7c, f), resulting in abundant water vapor and anomalous convergence over SC but reduced water vapor and anomalous divergence over YNC (Fig. 8c, f), leading to above-normal rainfall over SC (Fig. 4c) and below-normal rainfall over YNC (Fig. 4f). Such differences of the circulation and rainfall anomalies between in-phase and out-of-phase composites closely resemble the warm PDO-related circulation and rainfall anomalies shown by Wu and Mao (2016). The above analyses demonstrate that the circulation anomalies, as responses to ENSO-related SSTAs modified by PDO, could actually induce the first two EOF modes of spring rainfall anomalies over eastern China.

5 Simulation results

Finally, numerical simulations are performed to examine the influence of the SSTA forcing associated with the in-phase

and out-of-phase PDO–ENSO events. Figure 9a, b shows climatological distributions of simulated spring rainfall and 850-hPa winds in the CAM5-CTRL experiment. In comparison with JRA-55 products (Fig. 9c), CAM5 simulates reasonably well the major features of the spring persistent rainfall belt from southern China to southern Japan, although the maximum rainfall belt extends farther northward over eastern China (Fig. 9a). It also captures well the southwesterlies over East Asia from the WNP and south of the Tibetan Plateau, and the northwesterlies from mid-latitudes (Fig. 9b). Note that the southwesterlies are somewhat stronger and the northwesterlies are slightly weaker than those of JRA-55 (Fig. 9d). Having verified the control run, the differences between the CAM5-In-phase and CAM5-CTRL simulations are used to represent the in-phase composite anomalies, and the differences between CAM5-Out-of-phase and CAM5-CTRL for the out-of-phase composite anomalies.

The differences of simulated rainfall anomaly percentage between the CAM5-In-phase and CAM5-CTRL experiments (Fig. 10a) exhibit significantly positive anomalies over SC, in conjunction with insignificant weak negative anomalies over the

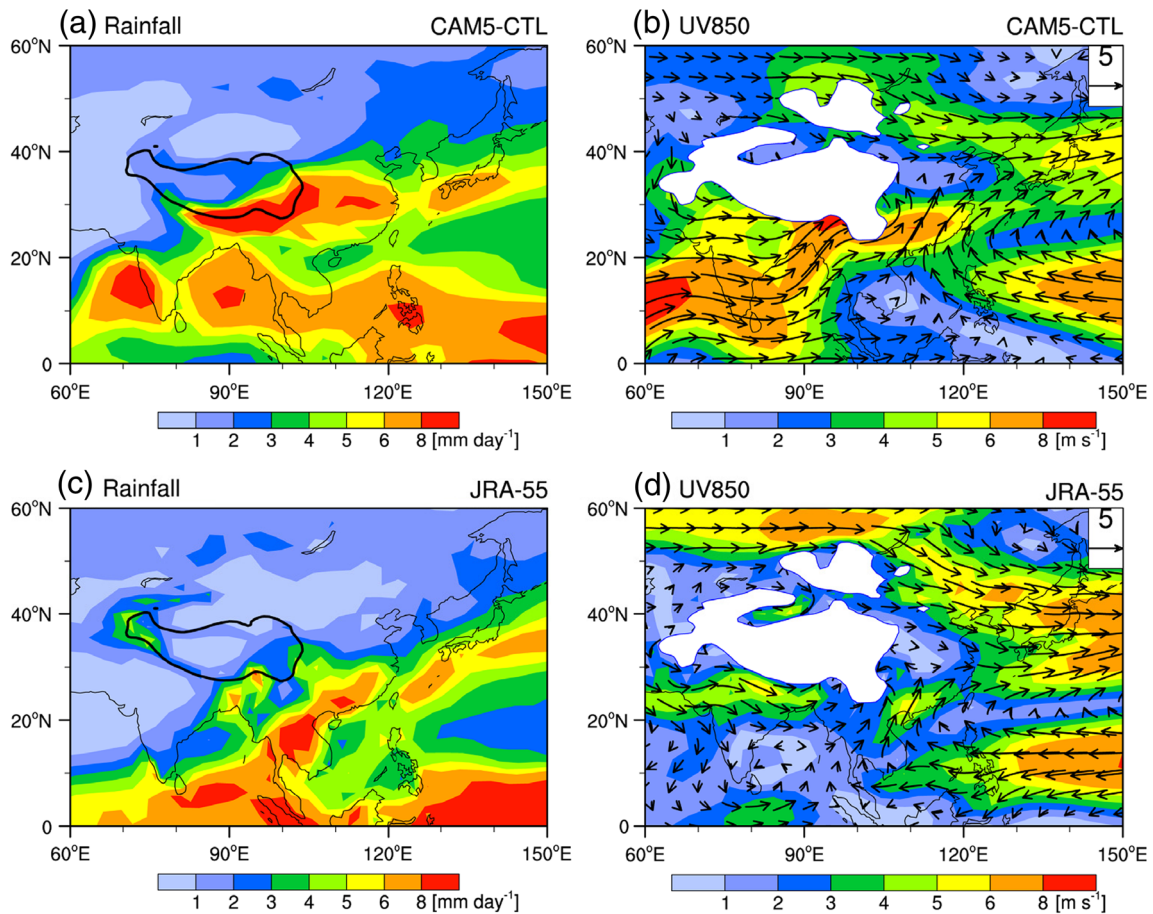


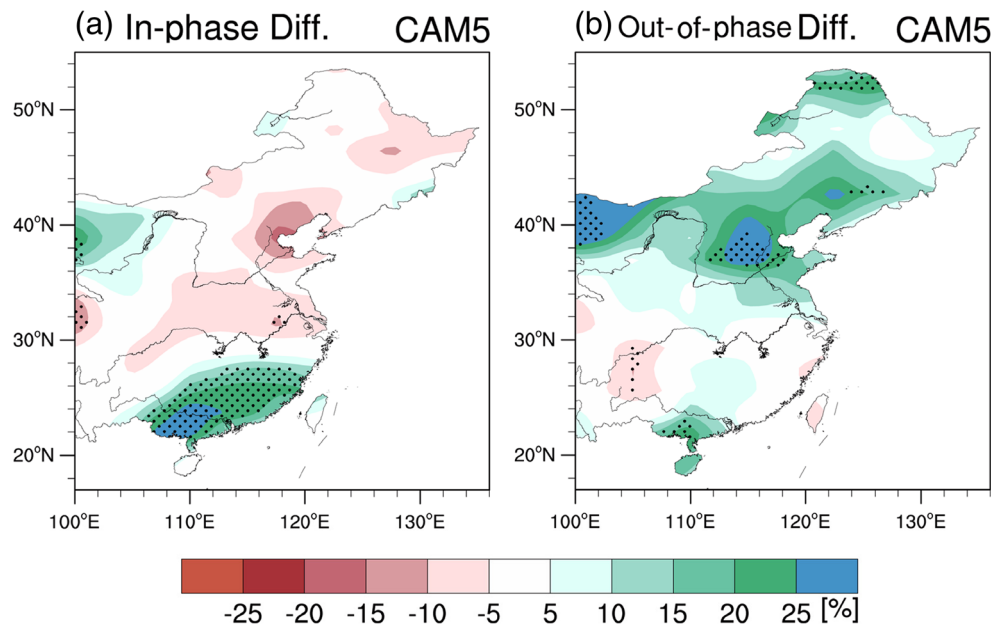
Fig. 9 Climatological distributions of the CAM5 simulated **a** spring rainfall (shading, mm day^{-1}) and **b** 850-hPa wind vectors (vectors, m s^{-1}) along with wind speeds (shading, m s^{-1}) derived from the 30-

year control experiment of CAM5 simulations (CAM5-CTRL). **c, d** Same as **a** and **b** but based on the JRA-55 reanalyses for the period 1958–2013

north of the Yangtze River, very similar to the in-phase composite rainfall anomalies (Fig. 4c) as indicated by the EOF2 pattern

(Fig. 2b). In response to the forcing by the SSTA pattern of EN_WPDO events, a southwest–northeast oriented dipole-like

Fig. 10 Composite differences of CAM5 simulated spring (March–May) rainfall anomaly percentage (color shading, %) **a** between CAM-In-phase and CAM5-CTRL experiments and **b** between CAM-Out-of-phase and CAM5-CTRL experiments. The stippling denotes the anomalies being statistically significant at the 95% confidence level



anomalous SLP pattern dominates the tropical and North Pacific, with significant positive SLP anomalies over the South China Sea and subtropical WNP, and strong negative SLP anomalies over the entire North Pacific (Fig. 11a). The simulated negative SLP anomalies also clearly extend southwestward to Japan, the Korean Peninsula, and eastern China, leading to southeastward contraction of the anomalous WNP anticyclone from eastern China. Anomalous southwesterlies prevail over SC (Fig. 11b), and lead to above-normal rainfall

over SC (Fig. 10a). Thus, the CAM5 simulations forced by EN_WPDO composite SSTAs reproduce well the EOF2 pattern of spring rainfall over eastern China as well as the circulation anomalies, indicating that the EOF2 is actually induced by the in-phase PDO–ENSO combinations, with EN_WPDO (LN_CPDO) events favoring positive (negative) rainfall anomalies over SC.

In contrast, the rainfall anomaly percentages of CAM5-Out-of-phase simulations exhibit significantly positive

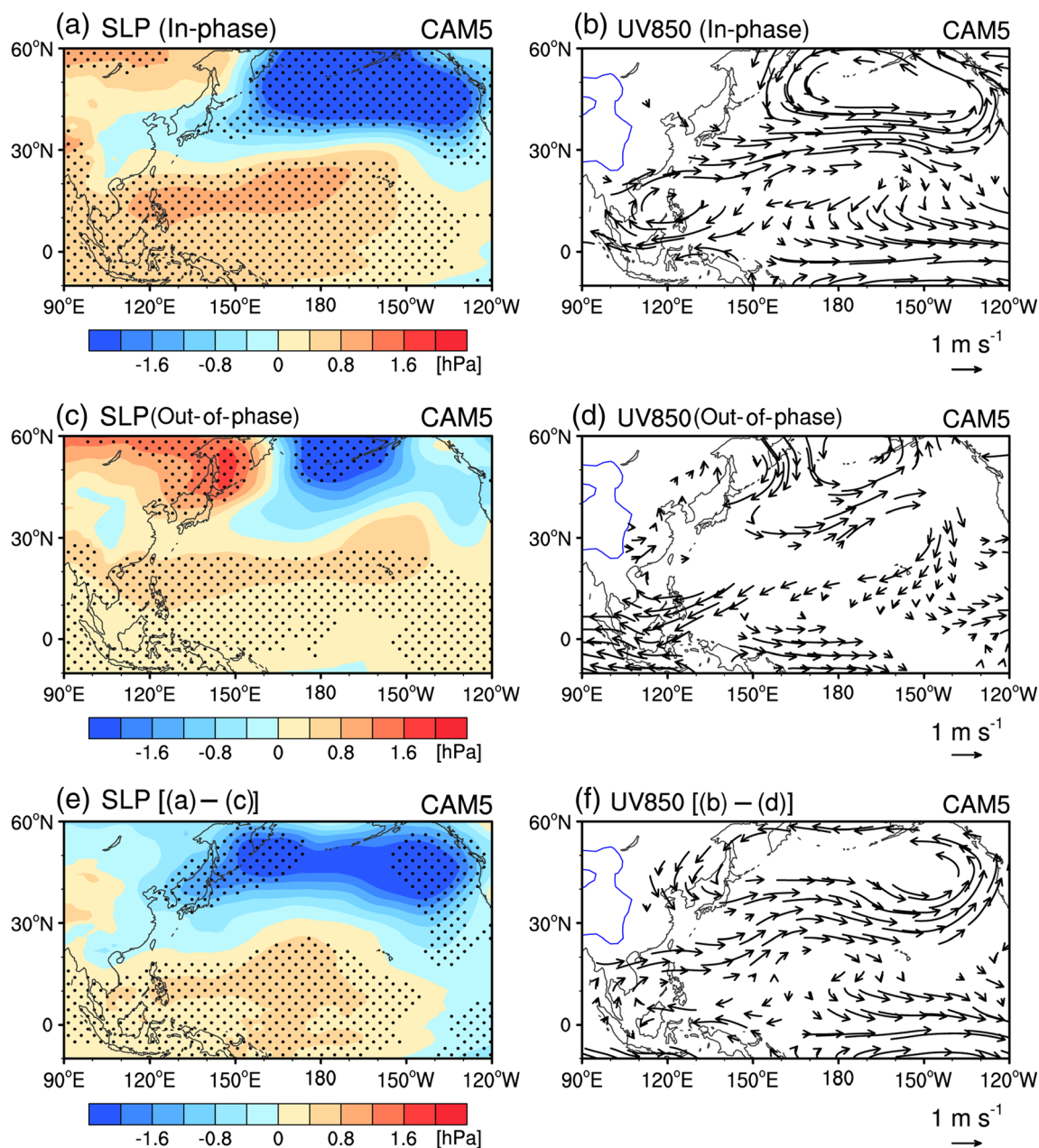


Fig. 11 Composites differences of CAM5 simulated spring (March–May) **a** SLP (shading, hPa) and **b** 850-hPa winds (vectors, m s^{-1}) between CAM5-In-phase and CAM5-CTRL experiments. The stippling in **a** denotes the anomalies being statistically significant at the 95% confidence level. Only shown in **b** are the vectors of which at least one

of the anomalous zonal and meridional wind components is statistically significant at the 95% confidence level. **c**, **d** and **e**, **f** are the same as **a**, **b**, but for the difference between CAM5-Out-of-phase and CAM5-CTRL experiments and the difference between CAM5-In-phase and CAM5-Out-of-phase experiments, respectively

anomalies over the middle and lower reaches of the Yellow River (Fig. 10b), capturing the major features of the EOF1 pattern (Fig. 2a), although the simulated rainfall anomalies are somewhat weaker than the observations over the regions between the Yangtze River and Yellow River. As a response to the EN_CPDO SSTAs, the simulated positive SLP anomalies over WNP extend northward over eastern China and north-eastward to the eastern North Pacific (Fig. 11c), although there is some overestimate of negative SLP near the Aleutian region. Associated with the realistic northward extension of the positive SLP anomalies over the WNP, the southwesterly anomaly prevailing over the major part of eastern China (Fig. 11d) is also simulated well, resulting in above-normal rainfall over the middle and lower reaches of the Yellow River (Fig. 10b). With forcing by the EN_CPDO SSTA pattern, the simulation can reproduce the major features of the EOF1 pattern of spring rainfall over eastern China and the circulation anomalies responsible for such rainfall anomalies. This confirms that the EOF1 mode is indeed related to the out-of-phase PDO–ENSO combinations, that is, the rainfall anomaly pattern of positive EOF1 usually follows EN_CPDO events while that of negative EOF1 follows LN_WPDO events.

The simulated southward shrinking of the WNP anomalous anticyclone in in-phase composites (Fig. 11a) and its northward extension in out-of-phase composites (Fig. 11c) are in good agreement with the observations (Fig. 7a, b), and the simulated circulation differences between in-phase and out-of-phase composites show typical features of a warm PDO, characterized by a dipole-like pattern with a zonally stretched anomalous anticyclone over the subtropical and equatorial western Pacific and an anomalous cyclone over the entire mid-latitude North Pacific and East Asia (Fig. 11e, f). This confirms that the anomalous anticyclone over the WNP is modified by the anomalous cyclone over the mid-latitude North Pacific and East Asia in association with PDO-related SST anomalies in the extratropical Pacific and further modulates the spring rainfall anomalies over eastern China.

6 Summary and discussion

The dominant spatial modes of spring rainfall anomalies over the entire area of eastern China and their interannual variability in relation to PDO–ENSO events are examined over the period 1920–2013, using the CMA station-observed monthly rainfall datasets and JRA-55 reanalysis products, as well as the long-term monthly CRU precipitation datasets and ERA-20C reanalysis products for cross validation. EOF analysis was performed to identify the spatio-temporal variations of spring rainfall over the entire eastern China. The first leading mode (EOF1) is dominated by positive anomalies over the middle and lower reaches of the Yellow River in YNC and is more likely associated with the out-of-phase PDO–ENSO events, with the EN_CPDO

(LN_WPDO) events being favorable for positive (negative) spring rainfall anomalies over YNC. The second leading mode (EOF2) is characterized by a north–south oriented dipole distribution with predominantly positive rainfall anomalies over SC and negative anomalies over the lower reaches of the Yellow River. This mode is more likely related to the in-phase PDO–ENSO events, with significant positive (negative) rainfall anomalies over SC following the EN_WPDO (LN_CPDO) events.

The physical mechanism relating different PDO–ENSO events to the interannual variability of the two dominant modes of spring rainfall over eastern China is via forced atmospheric teleconnections. Under in-phase PDO–ENSO situations, EN_WPDO events are characterized by significantly enhanced positive SSTAs over the central and eastern equatorial Pacific as well as enhanced negative SSTAs over the mid-latitude North Pacific, resulting from superposition of ENSO-related SSTAs on similar patterns of PDO-related SSTAs. Such strengthened SSTA patterns in turn force an enhanced anomalous cyclone over the mid-latitude North Pacific and a simultaneously enhanced anomalous anticyclone over the subtropical WNP. The southwestward extension of the enhanced PDO-related anomalous cyclone to the coastal regions of East Asia causes the low-level anomalous anticyclone over the WNP to contract southeastward to the southern portion of the South China Sea. As a result, the anomalous northeasterlies on the southern side of the anomalous cyclone prevail north of the Yangtze River and converge with the anomalous southwesterly induced by the contracted anomalous WNP anticyclone towards SC and the northern South China Sea. There is significant convergence of moisture flux over SC, resulting in significantly positive rainfall anomalies over SC along with somewhat negative rainfall anomalies north of the Yangtze River, corresponding to the positive distribution of spring rainfall anomalies described by the EOF2 pattern over eastern China, and vice versa for LN_CPDO events.

Following out-of-phase PDO–ENSO events, the superposition of ENSO-related SSTAs on the opposite patterns of PDO-related SSTAs mean that positive SSTAs during EN_CPDO events are only present over the central equatorial Pacific, accompanied by a belt of significantly positive SSTAs stretching from south of Japan to the central North Pacific. As a response to such an SSTA pattern, a weakened anomalous anticyclone exists over the WNP and extends northeastward to connect with the cold-PDO-associated anomalous anticyclone over the mid-latitude North Pacific. This anomalous WNP anticyclone also extends northward to Japan and the Korean Peninsula in response to the positive SSTA belt south of Japan. Consequently, anomalous southwesterlies prevail over the middle and lower reaches of the Yellow River, with strong convergence of water vapor flux, leading to above-normal rainfall over YNC, forming the positive distribution of spring rainfall anomalies seen in the EOF1 pattern over eastern China, and vice versa for LN_WPDO.

The simulation experiments with the CAM5 model forced by SSTA patterns of EN_WPDO (EN_CPDO) events reproduce well the spring rainfall anomaly pattern of the EOF2 (EOF1) mode. When forced by EN_WPDO SSTAs, the CAM5 simulation reproduces well the anomalous zonally stretched cyclone over the North Pacific and East Asia, which causes the anomalous WNP anticyclone to contract away from the coastal region of eastern China. Meanwhile, as a response to EN_CPDO SSTAs, the CAM5 simulation reproduces reasonably well the northward extension of the anomalous WNP anticyclone to the Korean Peninsula and southern Japan. Thus, the numerical simulations verify that the anomalous cyclone over the North Pacific in association with PDO-related SSTAs can modulate the influences of ENSO on spring rainfall over eastern China, through modifying the spatial pattern of the anomalous WNP anticyclone, resulting in the EOF1 (EOF2) rainfall anomaly pattern during out-of-phase (in-phase) PDO–ENSO events.

The present study focuses on the influence of interannual and interdecadal variability of SSTAs in the tropical Pacific and North Pacific on the spatio-temporal variations of spring rainfall over entire eastern China. Recently, the SSTAs in the Indian Ocean have been found to have a large impact on East Asian climate (Chen et al. 2013a; Feng et al. 2014b). As suggested by Feng et al. (2014b), the positive (negative) South Indian Ocean subtropical dipole usually induces below-normal (above-normal) spring rainfall over the middle to lower reaches of the Yangtze River and Yellow River. ENSO-related SSTAs in the Pacific can also influence the SSTAs in

the Indian Ocean through the atmospheric bridge (Alexander et al. 2002). Thus, to clarify the relative importance of SSTAs from the Pacific and Indian oceans in affecting the spring rainfall over eastern China, additional numerical experiments should be conducted including forcing by separate SSTAs over different ocean regions.

Acknowledgments This research was jointly supported by the National Basic Research Program of China (2014CB953902), SOA Program on Global Change and Air-Sea Interactions (GASI-IPOVAI-03), the Natural Science Foundation of China (91537103, 41705065, and 41375087), and the Priority Research Program of the Chinese Academy of Sciences (QYZDY-SSW-DQC018 and XDA11010402).

Appendix

Fisher’s exact test (Conover 1980)

	Column 1	Column 2	Column total
Row 1	<i>a</i>	<i>b</i>	<i>C</i> ₁ (<i>a</i> + <i>b</i>)
Row 2	<i>c</i>	<i>d</i>	<i>C</i> ₂ (<i>c</i> + <i>d</i>)
Row total	<i>R</i> ₁ (<i>a</i> + <i>c</i>)	<i>R</i> ₂ (<i>b</i> + <i>d</i>)	<i>N</i> (<i>a</i> + <i>b</i> + <i>c</i> + <i>d</i>)

N observations are summarized in the table above, whose row totals are fixed as *R*₁ and *R*₂, and column totals are fixed as *C*₁ and *C*₂. The exact distribution of the test statistics of this table is given by the hypergeometric distribution, as follows:

$$P(T_2 = a) = \begin{cases} \frac{\binom{a+b}{a} \binom{c+d}{c}}{\binom{n}{a+c}} = \frac{(a+b)!(c+d)!(a+c)!(b+d)!}{n!a!b!c!d!}, & a = 0, 1, \dots, \min(R_1, C_1) \\ 0, & a = \text{other} \end{cases}$$

Here, $\binom{n}{k}$ is the binomial coefficient and the symbol $!$ indicates the factorial operator.

Lower tailed test

$$H_0 : p_1 \geq p_2$$

$$H_1 : p_1 < p_2$$

where *p*₁ is the probability of an observation in row 1 being classified into column 1, *p*₂ is the probability of an observation in row 2 being classified into column 1, and *t*_{obs} is the observed value of *T*₂.

If $P(T_2 \leq t_{obs}) \leq \alpha$, reject *H*₀ at the level of significance α . Use this when there is a negative association between the variables.

Upper tailed test

$$H_0 : p_1 \leq p_2$$

$$H_1 : p_1 > p_2$$

If $P(T_2 \geq t_{obs}) \leq \alpha$, reject *H*₀ at the level of significance α . Use this when there is a positive association between the variables.

References

- Alexander MA, Blade I, Newman M, Lanzante JR, Lau NC, Scott JD (2002) The atmospheric bridge: the influence of ENSO teleconnections on air-sea interaction over the global oceans. *J Clim* 15(16):2205–2231. [https://doi.org/10.1175/1520-0442\(2002\)015<2205:TABTIO>2.0.CO;2](https://doi.org/10.1175/1520-0442(2002)015<2205:TABTIO>2.0.CO;2)
- An LJ, Ren FM, Li YJ, Li YP (2014) Study on characteristics of regional drought events over North China during the past 50 years. *Meteorol Mont* (in Chinese) 40:1097–1105
- Andreoli RV, Kayano MT (2005) ENSO-related rainfall anomalies in South America and associated circulation features during warm and cold Pacific Decadal Oscillation regimes. *Int J Climatol* 25(15):2017–2030. <https://doi.org/10.1002/joc.1222>
- Ashok KS, Behera K, Rao SA, Weng HY, Yamagata T (2007) El Niño Modoki and its possible teleconnection. *J Geophys Res* 112: C11007. <https://doi.org/10.1029/2006jc003798>
- Barnett TP, Pierce DW, Saravanan R, Schneider N, Dommenges D, Latif M (1999) Origins of midlatitude Pacific decadal variability. *Geophys Res Lett* 26(10):1453–1456. <https://doi.org/10.1029/1999GL900278>
- Chan JCL, Zhou W (2005) PDO, ENSO and the early summer monsoon rainfall over south China. *Geophys Res Lett* 32(8):L08810. <https://doi.org/10.1029/2004gl022015>
- Chen J, Wen Z, Wu R, Chen Z, Zhao P (2013a) Interdecadal changes in the relationship between southern China winter-spring precipitation and ENSO. *Clim Dyn* 43:1327–1338
- Chen W, Feng J, Wu R (2013b) Roles of ENSO and PDO in the link of the East Asian winter monsoon to the following summer monsoon. *J Clim* 26(2):622–635. <https://doi.org/10.1175/JCLI-D-12-00021.1>
- Conley AJ, Garcia R, Kinnison D, Lamarque JF, Marsh D, Mills M, Smith AK, Tilmes S, Vitt F, Morrison H (2012) Description of the NCAR community atmosphere model (CAM 5.0). NCAR technical note
- Conover WJ (1980) Practical nonparametric statistic. Wiley, New York
- Ding YH (1992) Summer monsoon rainfalls in China. *J Meteorol Soc Jpn* 70(1B):373–396. https://doi.org/10.2151/jmsj1965.70.1B_373
- Duan W, Song L, Li Y, Mao J (2013) Modulation of PDO on the predictability of the interannual variability of early summer rainfall over south China. *J Geophys Res-Atmos* 118(23):13008–13021. <https://doi.org/10.1002/2013JD019862>
- Efron B (1982) The jackknife, the bootstrap and other resampling plans. Capital City Press, Montpelier. <https://doi.org/10.1137/1.9781611970319>
- Feng J, Li J (2011) Influence of El Niño Modoki on spring rainfall over south China. *J Geophys Res* 116:D13102. <https://doi.org/10.1029/2010jd015160>
- Feng J, Wang L, Chen W (2014a) How does the East Asian summer monsoon behave in the decaying phase of El Niño during different PDO phases? *J Clim* 27(7):2682–2698. <https://doi.org/10.1175/JCLI-D-13-00015.1>
- Feng JQ, Yu LJ, Hu DX (2014b) Influence of Indian Ocean subtropical dipole on spring rainfall over China. *Int J Climatol* 34(4):954–963. <https://doi.org/10.1002/joc.3732>
- Gershunov A, Barnett TP (1998) Interdecadal modulation of ENSO teleconnections. *Bull Am Meteorol Soc* 79(12):2715–2725. [https://doi.org/10.1175/1520-0477\(1998\)079<2715:IMOET>2.0.CO;2](https://doi.org/10.1175/1520-0477(1998)079<2715:IMOET>2.0.CO;2)
- Gong DY, Wang SW (1998) Impact of ENSO on the seasonal rainfall in China. *J Nat Disaster* (in Chinese) 7:44–52
- Gu D, Philander SGH (1997) Interdecadal climate fluctuation that depend on exchanges between the tropics and the extratropics. *Science* 275(5301):805–807. <https://doi.org/10.1126/science.275.5301.805>
- Harris I, Jones PD, Osborn TJ, Lister DH (2014) Updated high-resolution grids of monthly climatic observations—the CRU TS3.10 dataset. *Int J Climatol* 34(3):623–642. <https://doi.org/10.1002/joc.3711>
- Hoaglin DC, Mosteller F, Tukey JW (1983) Understanding robust and exploratory data analysis. Wiley, New York
- Ihara C, Kushnir Y, Cane MA, De la Pena VH (2007) Indian summer monsoon rainfall and its link with ENSO and Indian Ocean climate indices. *Int J Climatol* 27(2):179–187. <https://doi.org/10.1002/joc.1394>
- Kao HY, Yu JY (2009) Contrasting eastern-Pacific and central-Pacific types of ENSO. *J Clim* 22(3):615–632. <https://doi.org/10.1175/2008JCLI2309.1>
- Kim JW, Yeh SW, Chang EC (2014) Combined effect of El Niño–Southern Oscillation and Pacific Decadal Oscillation on the East Asian winter monsoon. *Clim Dyn* 42(3–4):957–971. <https://doi.org/10.1007/s00382-013-1730-z>
- Kobayashi S et al (2015) The JRA-55 reanalysis: general specifications and basic characteristics. *J Meteorol Soc Jpn* 93(1):5–48. <https://doi.org/10.2151/jmsj.2015-001>
- Krishnamurthy L, Krishnamurthy V (2014) Influence of PDO on South Asian summer monsoon and monsoon-ENSO relation. *Clim Dyn* 42(9–10):2397–2410. <https://doi.org/10.1007/s00382-013-1856-z>
- Lau KM, Li MT (1984) The monsoon of East-Asia and its global associations—a survey. *Bull Am Meteorol Soc* 65(2):114–125. [https://doi.org/10.1175/1520-0477\(1984\)065<0114:TMOEAA>2.0.CO;2](https://doi.org/10.1175/1520-0477(1984)065<0114:TMOEAA>2.0.CO;2)
- Li J, Yu R, Yuan W, Chen H, Sun W, Zhang Y (2015) Precipitation over East Asia simulated by NCAR CAM5 at different horizontal resolutions. *J Adv Model Earth Syst* 7(2):774–790. <https://doi.org/10.1002/2014MS000414>
- Mantua NJ, Hare SR, Zhang Y, Wallace JM, Francis RC (1997) A Pacific interdecadal climate oscillation with impacts on salmon production. *Bull Am Meteorol Soc* 78(6):1069–1079. [https://doi.org/10.1175/1520-0477\(1997\)078<1069:APICOW>2.0.CO;2](https://doi.org/10.1175/1520-0477(1997)078<1069:APICOW>2.0.CO;2)
- Mao J, Chan JCL, Wu G (2011) Interannual variations of early summer monsoon rainfall over South China under different PDO backgrounds. *Int J Climatol* 31(6):847–862. <https://doi.org/10.1002/joc.2129>
- McPhaden MJ, Lee T, McClurg D (2011) El Niño and its relationship to changing background conditions in the tropical Pacific Ocean. *Geophys Res Lett* 38(15):L15709. <https://doi.org/10.1029/2011GL048275>
- North GR, Bell TL, Cahalan RF, Moeng FJ (1982) Sampling errors in the estimation of empirical orthogonal functions. *Mon Weather Rev* 110(7):699–706. [https://doi.org/10.1175/1520-0493\(1982\)110<0699:SEITEO>2.0.CO;2](https://doi.org/10.1175/1520-0493(1982)110<0699:SEITEO>2.0.CO;2)
- Power S, Casey T, Folland C, Colman A, Mehta V (1999) Inter-decadal modulation of the impact of ENSO on Australia. *Clim Dyn* 15(5):319–324. <https://doi.org/10.1007/s003820050284>
- Rasmusson EM, Carpenter TH (1982) Variations in tropical sea-surface temperature and surface wind fields associated with the Southern Oscillation /El Niño. *Mon Weather Rev* 110(5):354–384. [https://doi.org/10.1175/1520-0493\(1982\)110<0354:VITSST>2.0.CO;2](https://doi.org/10.1175/1520-0493(1982)110<0354:VITSST>2.0.CO;2)
- Rayner NA, Parker DE, Horton EB, Folland CK, Alexander LV, Rowell DP, Kent EC, Kaplan A (2003) Global analyses of sea surface temperature, sea ice, and night marine air temperature since the late nineteenth century. *J Geophys Res* 108(D14):4407. <https://doi.org/10.1029/2002JD002670>
- Rong YS, Duan LY, Xu M (2008) Analysis on climatic diagnosis of persistent drought in North China during the period from 1997 to 2002. *Arid Zone Res* (in Chinese) 25:842–850
- Stickler A, Brönnimann S, Valente MA, Bethke J, Sterin A, Jourdain S, Roucaute E, Vasquez MV, Reyes DA, Allan R, Dee D (2014) ERA-CLIM historical surface and upper-air data for future reanalyses. *Bull Am Meteorol Soc* 95(9):1419–1430. <https://doi.org/10.1175/BAMS-D-13-00147.1>
- Tang YM, Deng ZW, Zhou XB, Cheng YJ, Chen D (2008) Interdecadal variation of ENSO predictability in multiple models. *J Clim* 21(18):4811–4833. <https://doi.org/10.1175/2008JCLI2193.1>

- Tian SF, Yasunari T (1998) Climatological aspects and mechanism of spring persistent rains over Central China. *J Meteorol Soc Jpn* 76(1):57–71. https://doi.org/10.2151/jmsj1965.76.1_57
- Wan R, Wu G (2007) Mechanism of the spring persistent rains over southeastern China. *Sci China Earth Sci* 50(1):130–144. <https://doi.org/10.1007/s11430-007-2069-2>
- Wang B, Wu R, Fu X (2000) Pacific-East Asian teleconnection: how does ENSO affect East Asian climate? *J Clim* 13(9):1517–1536. [https://doi.org/10.1175/1520-0442\(2000\)013<1517:PEATHD>2.0.CO;2](https://doi.org/10.1175/1520-0442(2000)013<1517:PEATHD>2.0.CO;2)
- Wang L, Chen W, Huang R (2008) Interdecadal modulation of PDO on the impact of ENSO on the east Asian winter monsoon. *Geophys Res Lett* 35(20):L20702. <https://doi.org/10.1029/2008GL035287>
- Wang S, Huang J, He Y, Guan Y (2014) Combined effects of the Pacific Decadal Oscillation and El Niño–Southern Oscillation on global land dry–wet changes. *Sci Rep* 4:6651. <https://doi.org/10.1038/Srep06651>
- Wu R, Kirtman BP (2007) Observed relationship of spring and summer East Asian rainfall with winter and spring Eurasian snow. *J Clim* 20(7):1285–1304. <https://doi.org/10.1175/JCLI4068.1>
- Wu X, Mao J (2016) Interdecadal modulation of ENSO-related spring rainfall over South China by the Pacific Decadal Oscillation. *Clim Dyn* 47(9–10):3203–3220. <https://doi.org/10.1007/s00382-016-3021-y>
- Wu X, Mao J (2017) Interdecadal variability of early summer monsoon rainfall over South China in association with the Pacific Decadal Oscillation. *Int J Climatol* 37(2):706–721. <https://doi.org/10.1002/joc.4734>
- Wu R, Hu ZZ, Kirtman BP (2003) Evolution of ENSO-related rainfall anomalies in East Asia. *J Clim* 16(22):3742–3758. [https://doi.org/10.1175/1520-0442\(2003\)016<3742:EOERA>2.0.CO;2](https://doi.org/10.1175/1520-0442(2003)016<3742:EOERA>2.0.CO;2)
- Yoon J, Yeh SW (2010) Influence of the Pacific Decadal Oscillation on the relationship between El Niño and the Northeast Asian summer monsoon. *J Clim* 23(17):4525–4537. <https://doi.org/10.1175/2010JCLI3352.1>
- Zhang Y, Wallace JM, Battisti DS (1997) ENSO-like interdecadal variability: 1900–93. *J Clim* 10(5):1004–1020. [https://doi.org/10.1175/1520-0442\(1997\)010<1004:ELIV>2.0.CO;2](https://doi.org/10.1175/1520-0442(1997)010<1004:ELIV>2.0.CO;2)
- Zhang P, Liu Y, He B (2016) Impact of East Asian summer monsoon heating on the interannual variation of the South Asian High. *J Clim* 29(1):159–173. <https://doi.org/10.1175/JCLI-D-15-0118.1>
- Zheng F, Li J (2012) Impact of preceding boreal winter southern hemisphere annular mode on spring precipitation over south China and related mechanism. *Chin J Geophys-Chin* 55:3542–3557
- Zheng F, Li J, Wang L, Xie F, Li X (2015) Cross-seasonal influence of the December–February Southern Hemisphere Annular Mode on March–May meridional circulation and precipitation. *J Clim* 28(17):6859–6881. <https://doi.org/10.1175/JCLI-D-14-00515.1>
- Zhu YM, Yang XQ (2003) Relationship between Pacific Decadal Oscillation (PDO) and climate variability in China. *Acta Meteorol Sin (in Chinese)* 61:641–654
- Zuo ZY, Zhang RH (2012) The anomalies of spring rainfall in eastern China and its relation with tropical Pacific SST and Eurasian snow. *Chin J Atmos Sci (in Chinese)* 36:185–194
- Zuo ZY, Zhang RH, Wu BY, Rong XY (2012) Decadal variability in springtime snow over Eurasia: relation with circulation and possible influence on springtime rainfall over China. *Int J Climatol* 32(9):1336–1345. <https://doi.org/10.1002/joc.2355>